Author's Accepted Manuscript

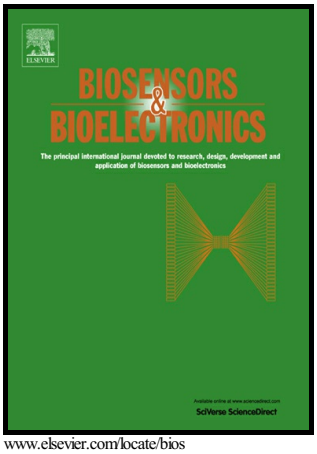

www.elsevier.com/locate/bios

Bioelectrocatalytic and Electrochemical Cascade for Phosphate Sensing with up to 6 Electrons per Analyte Molecule

Gabriel Kopiec, Karolina Starzec, Jolanta Kochana, Troy P. Kinnunen-Skidmore, Wolfgang Schuhmann, Wilbur H. Campbell, Adrian Ruff, Nicolas Plumeré

PII: S0956-5663(18)30479-2
DOI: https://doi.org/10.1016/j.bios.2018.06.047
Reference: BIOS10567

To appear in: *Biosensors and Bioelectronic*

Received date: 23 February 2018
Revised date: 9 June 2018
Accepted date: 24 June 2018

Cite this article as: Gabriel Kopiec, Karolina Starzec, Jolanta Kochana, Troy P. Kinnunen-Skidmore, Wolfgang Schuhmann, Wilbur H. Campbell, Adrian Ruff and Nicolas Plumeré, Bioelectrocatalytic and Electrochemical Cascade for Phosphate Sensing with up to 6 Electrons per Analyte Molecule, *Biosensors and Bioelectronic,* https://doi.org/10.1016/j.bios.2018.06.047

Bioelectrocatalytic and Electrochemical Cascade for Phosphate Sensing with up to 6 Electrons per Analyte Molecule

Gabriel Kopiec[a], Karolina Starzec[b], Jolanta Kochana[b], Troy P. Kinnunen-Skidmore[c], Wolfgang Schuhmann[d], Wilbur H. Campbell[c], Adrian Ruff*[d], Nicolas Plumeré*[a]

[a]*Center for Electrochemical Sciences (CES), Center for Electrochemical Sciences (CES), Ruhr-Universität Bochum, D-44780 Bochum, Germany*

[b]*Department of Analytical Chemistry, Faculty of Chemistry, Jagiellonian University, 30-060 Krakow, Poland*

[c]*The Nitrate Elimination Co., Inc. (NECi), Lake Linden, Michigan 49945, United States*

[d]*Analytical Chemistry, Center for Electrochemical Sciences (CES), Ruhr-Universität Bochum, D-44780 Bochum, Germany*

nicolas.plumere@rub.de

adrian.ruff@rub.de

*Corresponding Author. Phone: +49 234 3229434.
*Corresponding Author. Phone: +49 234 3225474.

ABSTRACT

Despite the availability of numerous electroanalytical methods for phosphate quantification, practical implementation in point-of-use sensing remains virtually nonexistent because of interferences from sample matrices or from atmospheric O_2. In this work, phosphate determination is achieved by the purine nucleoside phosphorylase (PNP) catalyzed reaction of inosine and phosphate to produce hypoxanthine which is subsequently oxidized by xanthine oxidase (XOx), first to xanthine and then to uric acid. Both PNP and XOx are integrated in a redox active Os-complex modified polymer, which not only acts as supporting matrix for the bienzymatic system but also shuttles electrons from the hypoxanthine oxidation reaction to the electrode. The bienzymatic cascade in this second generation phosphate biosensor selectively delivers four electrons for each phosphate molecule present. We introduced an additional electrochemical process involving uric acid oxidation at the underlying electrode. This further enhances the anodic current (signal amplification) by two additional electrons per analyte molecule which mitigates the influence of electrochemical interferences from the sample matrix. Moreover, while the XOx catalyzed reaction is sensitive to O_2, the uric acid production and therefore the delivery of electrons through the subsequent electrochemical process are independent of the presence of O_2. Consequently, the electrochemical process counterbalances the O_2 interferences, especially at low phosphate concentrations. Importantly, the electrochemical uric acid oxidation specifically reports on phosphate concentration since it originates from the product of the bienzymatic reactions. These advantageous properties make this bioelectrochemical-electrochemical cascade particularly promising for point-of-use phosphate measurements.

ABBREVIATIONS

PNP, purine nucleoside phosphorylase; XOx, xanthine oxidase; GCE, glassy carbon electrode; P-Os, poly(1-vinylimidazole-*co*-allylamine)-[Os(bpy)$_2$Cl]Cl; PEGDGE, poly(ethylene glycol) diglycidyl ether

KEYWORDS

Phosphate Biosensing, Xanthine Oxidase, Purine Nucleoside Phosphorylase, Point-of-Use Analysis, Redox Polymers, Enzyme Electrodes.

1. INTRODUCTION

The intensive and often excessive use of fertilization in agriculture results in major losses of soluble nutrients like phosphate ions into the ground water (Wittbrodt et al. 2015). As a consequence, undesirable biomass growth is accelerated in lakes and

coastal seas leading to depletion of oxygen levels in these water bodies with severe consequences for the natural environment (Duffy et al. 2017; Schindler 2012; Smith 2003). Fast and straightforward sensing tools are required by the famers to determine phosphate right before deploying the fertilizers for better input adjustment and hence limit the runoff into the groundwater. The classical colorimetric methods for the determination of phosphate (Fiske and Subbarow 1925) require strong acids, heavy metals or organic dyes which are not compatible with point-of-use field measurements and require time consuming sample preparation. Enzymatic methods may be better suited as analytical approaches for point-of-use phosphate analysis even in complicated sample matrices owing to their high selectivity as well as being non-toxic (Campbell et al. 2015). The coupling of enzymatic processes with electroanalytical methods are particularly promising for field sensing of nutrients such as nitrate (Plumeré et al. 2012) and phosphate because they open up the possibility for non-trained users to perform the analysis directly in the field without any sample preparation or specific pretreatment.

Although, electrochemical methods are well established for phosphate quantification (Barus et al. 2016; Berchmans et al. 2012; Grand et al. 2017; Jońca et al. 2011; Jońca et al. 2012; Jońca et al. 2013), point-of-use analysis was not described so far. Bioelectroanalytical phosphate sensing was previously proposed based on a bienzymatic system consisting of purine nucleoside phosphorylase (PNP) and xanthine oxidase (XOx) performing a cascade reaction (d'Urso and Coulet 1990; Haemmerli et al. 1990; Watanabe et al. 1988; Wollenberger et al. 1992). PNP catalyzes the reaction of inosine and phosphate to produce hypoxanthine which is subsequently oxidized by XOx, first to xanthine and then to uric acid. The use of PNP is especially advantageous due to its high selectivity. Campbell *et al.* tested in earlier studies typical constituents, i.e. metal ions and anions of soil (calcium, magnesium, sodium, iron, sulfate, chloride) and none of them were interfering when present at low levels (1 - 10 mM) (Campbell et al. 2015). Only arsenate (analog to phosphate) was found to be an interference for phosphate sensing. However, the concentration is usually in the ppb range and thus no significant effect on enzyme´s kinetics is expected. For XOx, specific flavonoids (especially compounds with a -OH group at the C7 position of the flavonoid core (Nagao et al. 1999)) can act as interferences and decrease the enzyme´s activity. Nevertheless, since the redox potential of many natural flavonoids are rather high (see e.g. (Jovanovic et al. 1996)) artefacts in the electrochemical measurements due to unintended oxidation of these compounds should be mostly suppressed.

Previous groups working on the bienzymatic XOx/PNP system took advantage of molecular oxygen as electron acceptor for the XOx catalyzed oxidation reactions in analogy to the first generation amperometric glucose biosensors (Wang 2008). The H_2O_2 generated from O_2 reduction by XOx is subsequently detected at the electrode and the resulting current is used for phosphate quantification (d'Urso and Coulet 1993; Kinoshita et al. 1995; Kulys et al. 1992; Male and Luong 1991). The general drawback of using O_2 as co-reactant in oxidase based sensors is that the quantification range is limited by the rather low concentration of dissolved oxygen in aqueous solutions (about 250 µM at 25 °C) (Zhang and Wilson 1993). Therefore, high phosphate concentrations, which are often found in soil or plant samples (in the mM range), require dilution steps that are major sources of error when performed on the field by untrained users.

The use of artificial electron acceptors, as pioneered for the so-called second generation amperometric glucose biosensors (Heller and Feldman 2008), renders the sensing independent of the presence of O_2 as co-reactant. This contributed to make the operation of electrochemical point-of-use devices suitable for end-users. These second generation biosensors generally rely on redox-active polymers which serve as electron relays between the redox-enzyme and the electrode surface and simultaneously provide a highly solvated immobilization matrix for the biocatalysts (Heller 1990; Ruff 2017). Previous reports have shown the immobilization of various oxidases, including XOx in second generation biosensors (Arai et al. 1996). Nevertheless, O_2 remains a problem in this type of biosensors. While the reaction between the oxidase and molecular oxygen becomes unnecessary, it still takes place since the oxidase reacts with O_2 as the natural electron acceptor. Hence, O_2 competes with the redox-active polymer for electrons generated by the oxidase (Mano et al. 2003). Moreover, O_2 may also be reduced by the redox-active polymer depending on its redox potential, which induces additional direct short-circuiting pathways (Bambhania et al. 2017; Lopez et al. 2018; Mano et al. 2005; Prévoteau and Mano 2012, 2013). Therefore, O_2 interferes by decreasing the current related to analyte oxidation and this issue is exacerbated for low analyte concentrations (Mano et al. 2003; Prévoteau and Mano 2012, 2013).

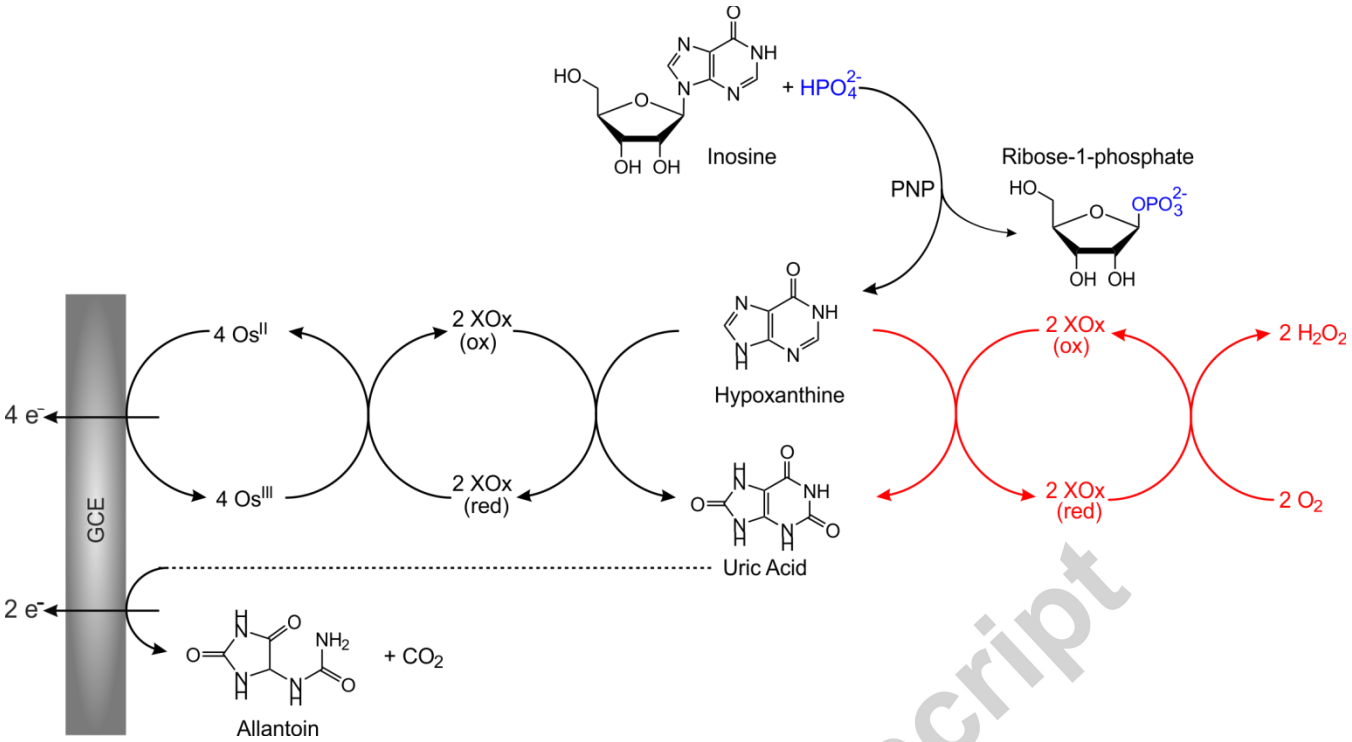

Scheme 1. Electrochemical phosphate sensing by means of PNP and XOx immobilized in an Os-complex modified hydrogel film on a glassy carbon electrode. Conversion of inosine and phosphate to ribose-1-phosphate and hypoxanthine catalyzed by PNP, followed by the 4-electron bioelectrocatalytic oxidation of hypoxanthine to uric acid via XOx and the subsequent 2-electron anodic oxidation of uric acid directly at the GCE; 4 electrons generated from the hypoxanthine oxidation can either be transferred via the $Os^{II/III}$-couple within the redox polymer to the electrode or be consumed by O_2 to produce hydrogen peroxide (red) under air. Since the product of the bienzymatic reactions is uric acid, which can be directly oxidized at the electrode, quantification of phosphate is still possible even under ambient air.

Various strategies have been proposed to circumvent the O_2 interference and thus enable the electrochemical sensing with oxidases in point-of-use analysis under ambient air. For instance, O_2 scavengers were successfully demonstrated for reductase-based sensors (Plumeré et al. 2012; Plumeré 2013; Quan et al. 2005) and may be applied likewise to oxidase-based sensors. Additionally, the film of the redox polymer containing the oxidase can be engineered in terms of film thickness (Grattieri et al. 2016), electron transfer rates (Mano et al. 2003) or redox potential (Pinyou et al. 2016; Prévoteau and Mano 2012) to minimize the competing O_2 reduction reaction. The oxidase can also be genetically modified toward lower O_2 reduction rates by site directed mutagenesis (Tremey et al. 2017) or co-factor redesign (Tremey et al. 2014). Moreover, the oxidase can also be replaced with a dehydrogenase (Chung et al. 1997; Gross et al. 2017; Milton et al. 2015; Shao et al. 2013; Tsujimura et al. 2014) that does not reduce O_2. However, these approaches are not suitable for all analytes and are often detrimental to sensor performances (Ferri et al. 2011). In particular, a solution to O_2 interferences in phosphate sensing with the PNP/XOx system has not been demonstrated until now.

Here, we propose to enhance the anodic signal related to phosphate detection in a second generation amperometric phosphate sensor to mitigate the O_2 interference. PNP and XOx are co-immobilized in an Os-complex modified polymer serving as an electron conducting matrix (Scheme 1). The electrons generated from the XOx catalyzed hypoxanthine oxidation are either transferred via the $Os^{II/III}$-couple to the electrode (catalytic current generation, denoted as $j_{cat}(1)$ in the following) or are consumed by O_2 to produce H_2O_2 (competing process (Martens et al. 1995; Martens and Hall 1994; Ohara et al. 1994)). Nevertheless, uric acid is produced from the biocatalyzed hypoxanthine oxidation irrespective of the nature of the electron acceptor (Os^{III} or O_2) and its electrochemical oxidation directly at the glassy carbon surface delivers additional 2 electrons for current generation (denoted as $j_{cat}(2)$). This process is independent of the presence of O_2 and secures, even for low phosphate concentration, an electrochemical signal that would otherwise fully vanish in presence of ambient air. Moreover, the enhanced signal generation through uric acid oxidation further mitigates the effect of other interferences that may be present in the sample matrix. Suppression of the interferences in phosphate sensing is the key to make the analytical procedure free of sample pre-treatment and thus makes the phosphate sensing practical for point-of-use analysis even in the hands of non-trained users.

2. EXPERIMENTAL SECTION

2.1 Instrumentation and Chemicals. All electrochemical experiments were conducted with the Gamry Reference 600 as potentiostat. The electrochemical cell consisted of a conventional three-electrode set-up with a cell volume of 5 mL. For all measurements, HEPES buffer (100 mM, pH 7.3) containing KCl (100 mM) was used as the electrolyte. For phosphate sensing, inosine (1 mM) was added to the electrolyte. The working electrodes were glassy carbon electrodes (GCE) from CHI (3 mm in diameter). The reference electrode consisted of an Ag/AgCl/KCl (3 M) system. A platinum wire (1.0 mm in diameter) served as the counter electrode. All potentials were rescaled to the standard hydrogen electrode (SHE). Phosphate calibration experiments were executed using 0.1 mM, 1 mM and 10 mM stock solutions. Dried forage samples were ground to fine powder with mortar and pestle. The sample (1 g in 20 mL ultrapure water) was filtered through Miracloth®. After filtration 16.2 mL were recovered, aliquoted and freeze dried. The freeze-drying step was performed to enable storage of the samples. For forage sample analysis, a freeze dried aliquot (corresponding to 100 µL of forage solution before freeze-drying) was dissolved in 500 µL of HEPES buffer (100 mM, pH 7.3) containing KCl (100 mM) resulting in a dilution factor of 5. The colorimetric assay of the phosphate content in the forage sample was performed according to protocols reported in ref (Campbell et al. 2015).

XOx (from cow milk; 1 U mg^{-1}), inosine, hypoxanthine and uric acid were purchased from Sigma Chemical Co. (St. Louis, MO) and recombinant *Escherichia coli* PNP was received from NECi Superior Enzymes (nitrate.com). The Os-complex modified polymer poly(1-vinylimidazole-*co*-allylamine)-[Os(bpy)$_2$Cl]Cl (P-Os) was synthesized according to protocols reported in ref (Sokol et al. 2016). However, an additional purification step was introduced after the modification of the polymer backbone with the Os-complex to obtain the pure redox polymer as an aqueous solution (see Supporting Information for a detailed description of the synthesis). All other chemicals are of reagent grade. All aqueous solutions were prepared using water from Milli-Q water purification system.

2.2 Electrode Modification. GCEs were polished on polishing cloth with decreasing sizes of alumina suspensions (1, 0.3, 0.05 µm, Leco) and subsequently sonicated for 10 min in ethanol/water (1:1) prior to modification. Several polymer-enzymes-crosslinker ratios were tested with respect to high current response and high stability. The best ratio was found to be 44.5 wt% (P-Os), 35.6 wt% (XOx), 8.9 wt% (PNP) and 11.0 wt% (PEGDGE). The electrodes were modified in a standard drop-casting process as follows: A droplet (2.63 µL) of the polymer solution (4 µg $µL^{-1}$) was mixed together with aqueous solutions of XOx (0.36 µL, 23.4 µg $µL^{-1}$) and PNP (0.21 µL, 10 µg $µL^{-1}$), drop-cast on the electrode surface and stored for 1 day at 8 °C in the fridge to let it dry slowly. Afterwards, the electrode was treated with 1.3 µL of poly(ethylene glycol) diglycidyl ether (PEGDGE) (2 µg $µL^{-1}$) as well as 3 µL of Tris-Cl buffer (pH 9) and left to dry for further 2 h under ambient air (Kothe et al. 2014). The specific concentration of the polymer, enzymes and crosslinker on the electrode surface (0.07 cm^{-2}) was calculated to be 150 µg cm^{-2} (P-Os), 120 µg cm^{-2} (XOx), 30 µg cm^{-2} (PNP) and 37 µg cm^{-2} (PEGDGE).

3. RESULTS AND DISCUSSION

For the immobilization of the bienzymatic PNP/XOx system, we used an Os-complex modified poly(vinylimidazole-*co*-allylamine) based polymer (P-Os, Fig. S1). Cyclic voltammetry of glassy carbon electrodes modified with the P-Os/PNP/XOx films shows a reversible wave with a mid-point potential at +0.42 V vs. SHE attributed to the Os^{II}/Os^{III} interconversion (Fig. 1, black trace, see Fig. S2 for a cyclic voltammogram of the pristine polymer layer). Thus, the formal redox potential of P-Os is sufficiently high to ensure that reduction of O_2 at the P-Os can be neglected (Prévoteau and Mano 2012).

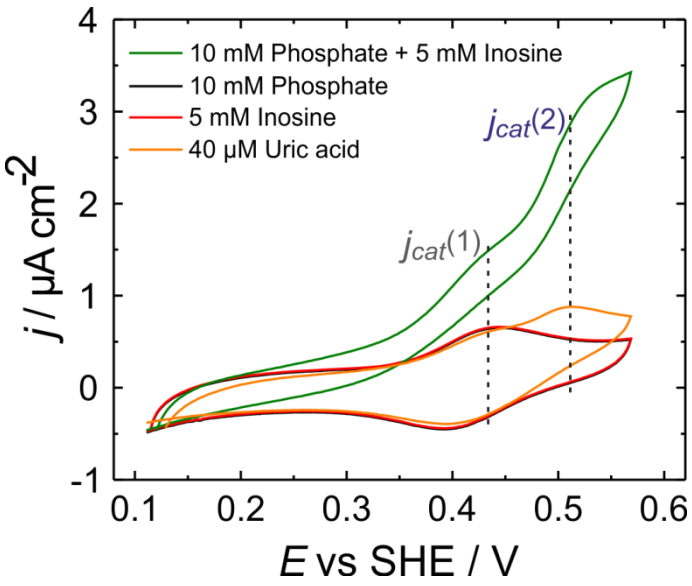

Fig. 1. Cyclic voltammograms recorded with a P-Os/PNP/XOx modified GCE in electrolyte containing 10 mM phosphate (black trace), in electrolyte containing 5 mM inosine (red trace), in electrolyte containing 5 mM inosine and 10 mM phosphate (green trace) and in electrolyte containing 40 µM uric acid (orange trace). For the definition of $j_{cat}(1)$ and $j_{cat}(2)$, see main text. All measurements were recorded at 2 mV s^{-1} under air in HEPES (100 mM, pH 7.3) with KCl (100 mM) acting as electrolyte. Specific surface concentrations of polymer, enzymes and crosslinker: 150 µg cm^{-2} (P-Os), 120 µg cm^{-2} (XOx), 30 µg cm^{-2} (PNP) and 37 µg cm^{-2} (PEGDGE).

The addition of both inosine and phosphate generates a two-step catalytic wave at a P-Os/PNP/XOx modified GCE (Fig. 1, green trace) with the half wave potential of the first wave ($j_{cat}(1)$) roughly centered on the mid-point potential of the Os^{II}/Os^{III} couple. If only inosine (Fig. 1, red trace) or only phosphate (black curve) is present, a non-catalytic signal identical to the one observed in pure electrolyte is obtained. Similarly, measurements in presence of both phosphate and inosine with films lacking both enzymes (Fig. S3) or containing only XOx (Fig. S4) lead to the non-catalytic wave due to the reversible oxidation of P-Os. All these observations are consistent with the enzyme cascade involving first generation of hypoxanthine through phosphorolysis of inosine to ribose-1-phosphate catalyzed by PNP, followed by the oxidation of hypoxanthine by XOx with electron transfer to the electrodes through the Os-complexes within P-Os as depicted in Scheme 1. This is further supported by the catalytic current obtained for films containing XOx in presence of hypoxanthine (Fig. S4, green trace) which is qualitatively comparable to the one observed for P-Os/PNP/XOx modified GCE in presence of both phosphate and inosine (Fig. 1).

The second wave ($j_{cat}(2)$), observed at more positive potentials, is attributed to an additional anodic process resulting from the 2-e^- oxidation of uric acid, which is the product of the XOx catalyzed 4-e^- hypoxanthine oxidation, at the underlying GCE. This is corroborated by the anodic current observed at a peak potential at about +0.52 V vs. SHE for electrodes modified with P-Os/PNP/XOx (Fig. 1, orange trace) upon addition of uric acid to the electrolyte. The peak potential value is in agreement with the position of $j_{cat}(2)$ and with the values reported for uric acid oxidation at bare glassy carbon electrodes (Wang and Tong 2010). In comparison, the redox potential of the $Os^{II/III}$-redox couple ($E^{0'}$= +0.42 V vs. SHE, see also Fig. S2c) is considerably less positive and therefore, does not contribute to the uric acid oxidation process. Moreover, hypoxanthine is not oxidized in this potential window if XOx is absent (Fig. S3, green trace), and xanthine is reported to be oxidized at much higher potentials on bare GCE (+0.95 V vs. SHE) (Wang and Tong 2010). Furthermore, forced convection imposed by stirring of the solution suppresses the current of the second wave (Fig. S5), which is consistent with the local production of the uric acid from hypoxanthine oxidation within the P-Os/PNP/XOx films and its depletion in front of the electrode upon stirring. Thus, the second wave in the catalytic current obtained under stationary conditions in presence of phosphate and inosine at P-Os/PNP/XOx modified GCE can be unambiguously attributed to the anodic oxidation of uric acid directly at the GCE.

Both $j_{cat}(1)$ and $j_{cat}(2)$ display similar shapes. Since uric acid is not present in the bulk of the solution, its flux to the electrode and thus the current response for its oxidation ($j_{cat}(2)$) is directly defined by its rate of generation within the film. At high phosphate concentration at which enzymatic activity is limiting, $j_{cat}(1)$ tends toward a plateau from which $j_{cat}(2)$ leads to a second plateau (Fig. 1) due to the steady state generation of uric acid. At low phosphate concentration at which mass transport of phosphate limits the catalytic current, $j_{cat}(1)$ has a peak shape (planar semi-infinite diffusion of phosphate from the bulk of the solution) followed by the equally peak-shaped response of $j_{cat}(2)$ (Fig. S6). These observations confirm that the processes responsible for $j_{cat}(2)$and $j_{cat}(1)$ are coupled.

The applicability of the P-Os/PNP/XOx modified electrodes for phosphate sensing was further investigated by cyclic voltammetry. In a point-of-use device, constant potential amperometry would be more practical for analyte quantification. However, we deliberately chose cyclic voltammetry for our study to elucidate the sensing mechanism and to study the effect of oxygen on the processes leading to $j_{cat}(1)$ and $j_{cat}(2)$. Cyclic voltammetry allows the analysis of both current responses under identical conditions within a single experiment. Phosphate sensing is in principle possible either at the first or at the second current wave as demonstrated by the correlation between the phosphate concentration with both $j_{cat}(1)$ and $j_{cat}(2)$ (Fig. 2). The upper limit of the quantification range is about 250 µM phosphate for both current waves irrespective of the presence of air (under argon: Fig. 2A; under air: Fig. 2B). The catalytic currents reach a plateau for phosphate concentration in the mM range. The same experiment repeated in a constant potential amperometric mode leads to the same result (Fig. S7). An increase in concentration of the inosine co-reactant from 1 to 50 mM results in comparable current responses at high phosphate concentrations (Fig. S6). Therefore, limitation in co-reactant availability, as usually observed in first-generation biosensors depending on the concentration of the natural electron acceptor O_2, is not defining the linear range here. Instead, the upper limit of the phosphate quantification range is attributed to the relatively low K_M value of PNP for phosphate which is about 135 µM (Lee et al. 2001). The fact that the co-reactant is not limiting the current is important since it opens up the possibility for a wider quantification range by using coulometric instead of voltammetric (or amperometric) measurements. In the latter case, the detectable current is limited by enzyme kinetics, diffusion of substrate and/or electron transport. Under coulometric conditions, the upper limit of the linear range can be extended by increasing the duration of the electrolysis until full conversion of the analyte present in the sample volume. Therefore, the direct quantification of phosphate even in highly concentrated samples would in principle be accessible with this second generation biosensor concept based on PNP/XOx upon proper design of a suitable sensing strip (low volume) for coulometric measurement procedures.

Of particular importance for point-of-use phosphate sensing is the impact of O_2 on the current response. Under both anaerobic and aerobic conditions, the background corrected current response displays a relatively larger $j_{cat}(2)$ compared to $j_{cat}(1)$ (Fig. 2A and 2B). However, the effect is more pronounced in presence of O_2 (Fig. 2A). These observations are in line with the proposed mechanism depicted in Scheme 1 involving the diversion of electrons from hypoxanthine oxidation at XOx by O_2. The short-circuiting of electrons by O_2 lowers $j_{cat}(1)$ while the contribution from the oxidation of uric acid to $j_{cat}(2)$ is not affected since the latter is produced also when O_2 serves as electron acceptor for XOx. Nevertheless, at high phosphate concentration the difference remains moderate and does not significantly impede the sensing performances.

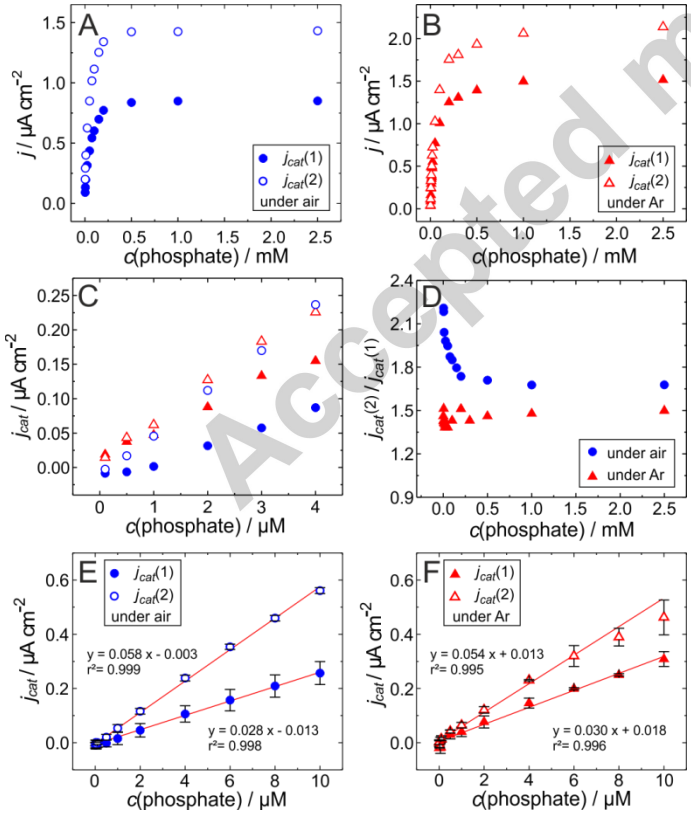

Fig. 2. Effect of phosphate concentrations and O_2 on catalytic current for P-Os/PNP/XOx modified GCEs. Background corrected catalytic currents at $j_{cat}(1)$ and $j_{cat}(2)$ vs. phosphate concentration (A) under air and (B) under argon. The corresponding CVs are given in Fig. S8A and S8B, respectively. (C) Effect of O_2 on catalytic currents at $j_{cat}(1)$ and $j_{cat}(2)$ for phosphate concentrations. The corresponding CVs are given in Fig. S8C and S8D. (D) Ratio of $j_{cat}(2)$ to $j_{cat}(1)$ under air and argon (data extracted from panels A and B). Calibration graphs for phosphate (E) under air and (F) under argon; j_{cat} values are averages of three independent cyclic voltammetry measurements; error bars represent standard deviations. All measurements were recorded at 2 mV s^{-1} in presence of 1 mM inosine in HEPES (100 mM, pH 7.3) with KCl (100 mM) acting as electrolyte. All data points measured in air are given in blue and all data points measured under argon are given in red. The closed symbol corresponds to $j_{cat}(1)$ and the open symbol to $j_{cat}(2)$. Specific surface concentrations of polymer, enzymes and crosslinker: 150 µg cm^{-2} (P-Os), 120 µg cm^{-2} (XOx), 30 µg cm^{-2} (PNP) and 37 µg cm^{-2} (PEGDGE).

At low phosphate concentration the impact of O_2 interference becomes severe. While under argon, the linear range reaches phosphate concentrations down to 0.5 µM at $j_{cat}(1)$ (Fig. 2C, red filled triangles), the catalytic current at $j_{cat}(1)$ in the presence of air is fully absent up to 1 µM (Fig. 2C, blue filled circles) and remains significantly lower in the 1 to 4 µM range. This results from the competitive $XOx_{(red)}$ oxidation (Scheme 1) which is at low phosphate concentrations largely in favor of the reaction with O_2 to produce H_2O_2 over the current generation through electron transfer via the $Os^{II/III}$-couple to the electrode. These results are in good agreement with theoretical models (Martens et al. 1995) and experimental results (Prévoteau and Mano 2013) reported for glucose sensing with glucose oxidase entrapped in Os-complex modified polymers which suffer from the same competitive process. In the case of phosphate sensing, the hypoxanthine oxidation via XOx and the subsequent uric acid oxidation, which is independent of the presence of O_2, opens the possibility to extend the detection limit to lower concentrations. At $j_{cat}(2)$, which includes the additional current contribution from uric acid oxidation, a linear behavior is obtained down to sub-micromolar phosphate concentrations even in presence of air (Fig. 2C, aerobic case: blue, anaerobic case: red). The advantage of using $j_{cat}(2)$ for phosphate sensing is highlighted by plotting the ratio $j_{cat}(2)$ / $j_{cat}(1)$ as a function of the phosphate concentration (Fig. 2D). The theoretical ratio between $j_{cat}(2)$ (2-e^- process overlapping with the 4 electron process of $j_{cat}(1)$) and $j_{cat}(1)$ (4-e^- process) is 1.5. Under anaerobic conditions, the experimental value for this ratio is in excellent agreement with the theoretical value and is independent of the phosphate concentration (Fig. 2D, red triangles). The value of 1.5 for this ratio also indicates that the uric acid generated within the film is almost quantitatively oxidized at the electrode. Loss of uric acid to the bulk of the solution is negligible since it is generated close to the electrode leading to a steep concentration gradient toward the electrode.

Table 1. Limit of detection[a] (LOD) for $j_{cat}(1)$ and $j_{cat}(2)$.

	$j_{cat}(1)$	$j_{cat}(2)$
LOD(argon) / µM	1.22	0.32
LOD(air) / µM	1.51	0.35

[a]LOD = 3 S_a/b; S_a= standard deviation of low concentration, b = slope of calibration curve. LOD values extracted from Fig. 2E and 2F.

However, for measurements performed under air, the ratio increases with decreasing phosphate concentrations (Fig. 2D, blue circles) since a fraction of the 4 electrons per phosphate molecule contributing to $j_{cat}(1)$ are taken by O_2. Therefore, the additional uric acid oxidation contribution to $j_{cat}(2)$ compensates for the signal loss due to O_2 at low concentration. The impact on the detection limit was quantified from the standard deviation at low phosphate concentrations and from the slope of the linear range of the calibration curves (Fig. 2E and 2F). Under air, the limit of detection obtained at $j_{cat}(1)$ is 1.51 µM which is about 25 % higher than the value obtained under argon (Table 1). At $j_{cat}(2)$ under air, the limit of detection decreases to 0.35 µM which is comparable to the value obtained under argon. This demonstrates that the additional uric acid oxidation is potentially advantageous to cancel out the interference from oxygen at low analyte concentrations in point-of-use phosphate sensing.

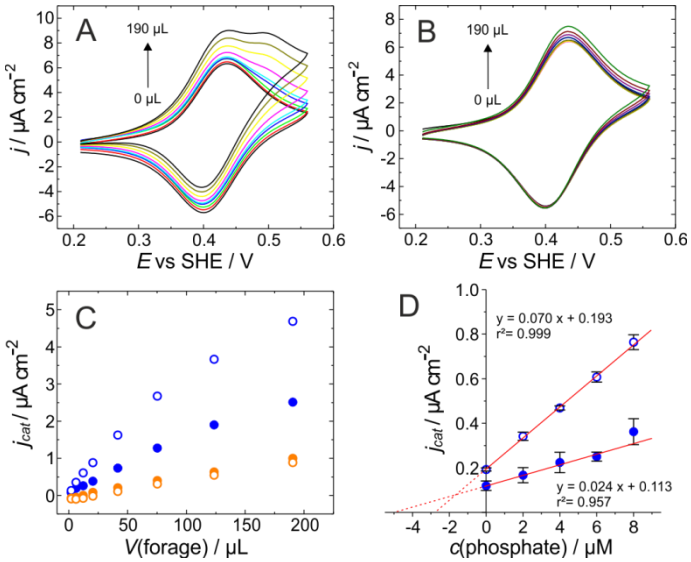

Fig. 3. Determination of the phosphate content in forage samples under air. Cyclic voltammograms recorded with P-Os/PNP/XOx modified GCE containing 1 mM inosine (A) and in absence of inosine (B). Increasing volumes of dissolved/suspended forage samples added in the range of 0 to 190 µL to a 1 mL electrolyte solution. Current densities for $j_{cat}(1)$ and $j_{cat}(2)$ extracted from the CVs of panels A and B (C). Current densities for $j_{cat}(1)$ and $j_{cat}(2)$ obtained from the standard addition method (D). The mean values and standard deviations were derived from three replicates with 3 different electrodes. Freeze dried forage was treated with 500 µL of HEPES (100 mM, pH 7.3) containing KCl (100 mM). Standard addition measurements were performed in 5 mL of HEPES (100 mM, pH 7.3) with KCl (100 mM) at 2 mV s^{-1} under air containing 20 µL of the diluted forage sample. All data points measured in presence of inosine are given in blue and all data points measured in absence of inosine are given in orange. The closed symbol corresponds to $j_{cat}(1)$ and the open symbol to $j_{cat}(2)$. Error bars indicate standard deviation. All measurements were conducted under ambient conditions. Specific surface concentrations of polymer, enzymes and crosslinker: 150 µg cm^{-2} (P-Os), 120 µg cm^{-2} (XOx), 30 µg cm^{-2} (PNP) and 37 µg cm^{-2} (PEGDGE).

We measured the electrochemical response of forage samples to test the impact of interferences from the sample matrix under ambient conditions. In a first step, a blank GCE (Fig. S9A) as well as the P-Os/PNP/XOx modified GCE (Fig. S9B) were used to measure the background current response from concentrated forage samples in absence of the inosine co-reactant. In both cases, an anodic current is obtained at potentials higher than +0.35 V vs. SHE. Since inosine was not used, this current is independent of the phosphate content and can therefore be assigned to the forage sample matrix that undergoes an electrochemical process at the GCE. Because of its relatively low onset potential, this process may in principle interfere with both $j_{cat}(1)$ and $j_{cat}(2)$. In the next step the experiment was repeated in presence of inosine for the P-Os/PNP/XOx modified GCE to evaluate the contributions from the phosphate content with respect to the one of the sample matrix. The measurements were performed with diluted forage samples to remain in the amperometric linear range of the P-Os/PNP/XOx modified GCE. Cyclic voltammograms reveal the two current waves $j_{cat}(1)$ and $j_{cat}(2)$ (Fig. 3A) which are qualitatively comparable to the one observed for measurements with standard phosphate solutions (Fig. S8). The measurements were repeated in absence of inosine (Fig. 3B). Under these diluted conditions, the current due to the oxidation of the sample matrix are comparatively low. Nevertheless quantitative comparisons show that at $j_{cat}(1)$ the current contribution from the matrix is about 30 % of the total current (Fig. 3C, closed symbols). Hence, the matrix interferes significantly with the phosphate determination at this potential. In contrast, at $j_{cat}(2)$ the contribution from the matrix is only 10 % (Fig. 3C, open symbols). This highlights the benefit of using $j_{cat}(2)$ instead of $j_{cat}(1)$ for phosphate determination in forage samples not only to bypass the interference of O_2, but also to mitigate the interferences from the sample matrix owing to the current enhancement provided by the additional 2-e^- from uric acid oxidation.

Table 2. Phosphate concentrations[a] in forage samples determined by the electrochemical biosensor under air and by a standard colorimetric assay (Campbell et al. 2015).

Electrochemical	$j_{cat}(1)$	$j_{cat}(2)$
From calibration[b] / mM	3.99± 0.74	2.73 ± 0.16
From standard addition[c] / mM	5.76 ± 0.64	3.43 ± 0.13
Colorimetric[d] / mM	3.18 ± 0.51	

[a] The mean values and standard deviations are obtained from at least 3 independent measurements. [b] The calibration curve is given in Fig. 2E and the measurements are given in Fig. S10. [c] The measurements are given in Fig. 3D. [d] The measurements are given in Fig. S11.

The phosphate concentration was determined from the current response in the voltammetric measurements in presence of inosine under ambient air (Fig. S10) by using the calibration curve (Fig. 2E) as well as the standard addition method (Fig. 3D). The phosphate concentrations obtained from the electrochemical methods at both $j_{cat}(1)$ and $j_{cat}(2)$ were compared with the values obtained from a standard colorimetric method (Campbell et al. 2015) (Table 2). The phosphate concentration values obtained from $j_{cat}(1)$ are about 50 % more than the ones obtained from $j_{cat}(2)$. The results are similar whether the phosphate determination is based on the calibration curve or based on the standard addition method. However, the values obtained from $j_{cat}(2)$ are in excellent agreement with those obtained from colorimetric measurements (Table 2). This confirms the advantage of using $j_{cat}(2)$ to minimize interferences from both O_2 and the sample matrix. It should also be mentioned that the possibility to perform blank measurements by omitting inosine as co-reactant could be used to further increase the accuracy of the measurements by subtracting the sample matrix contribution. The practicability of this approach is in principle compatible with point-of-use phosphate sensing.

The stability of the P-Os/PNP/XOx modified GCE was tested for multiple measurements. While on the time scale of hours, several consecutive measurements are possible, overnight storage in a buffer solution results in almost complete loss of the current signal (Fig. S12). Evidently, the phosphate sensing concept is not suitable for application involving multiple or continuous phosphate measurements. However, when the P-Os/PNP/XOx modified GCE are stored dried before use, the impact on the catalytic current was negligible even for storage up to several days. This storage stability parameter is most important regarding the application as single-use sensors envisioned for point-of-use phosphate analysis.

4. CONCLUSION

The bienzymatic system combining PNP and XOx embedded in an Os-complex modified polymer on a glassy carbon electrode surface generates a current response in form of a two-step oxidation wave in presence of phosphate and inosine. We demonstrate that the first wave is due to the bioelectrocatalytic oxidation of hypoxanthine generated from the phosphorolysis of inosine, whereas the second wave originates from the direct oxidation of uric acid, the product of hypoxanthine oxidation, at the electrode surface. Both waves are suitable for electrochemical phosphate sensing under anaerobic conditions. However, we show that the 4 electrons generated from the hypoxanthine oxidation can be consumed by oxygen at the xanthine oxidase and thus decreases or fully cancels the catalytic current. The uric acid oxidation directly at the electrode surface is beneficial to compensate for the competitive hypoxanthine oxidation by an additional 2-electron process that yield performances in presence of air approaching the one obtained under argon. Additionally, the resulting current enhancement also mitigates other possible interferences present in the sample matrix. This makes this sensing concept particularly suitable for point-of-use phosphate measurements since it bypasses the need for sample pretreatment. This bioelectrocatalytic/electrochemical cascade may be transposed to other sensing concept involving XOx such as hypoxanthine or xanthine biosensing and warrants the reliable quantification of the analyte even in the presence of interfering O_2, which usually limits the use of oxidase based sensors in point-of-use devices. Ultimately, the integration of this sensor concept into small volume sensing strip that can be operated in the coulometric mode will enable calibration-free and dilution-free procedures to enable reliable point-of-use phosphate sensing.

ACKNOWLEDGMENT

This work was supported by the Cluster of Excellence RESOLV (EXC 1069) funded by the Deutsche Forschungsgemeinschaft (DFG) and by the European Research Council (ERC Proof of Concept Grant 790155). We thank the United States Department of Agriculture NIFA program for SBIR grant #2018-00638 to WHC. We would also like to thank Melinda Nolten for the help with the synthesis of the Os-modified polymer.

References

Arai, G., Takahashi, S., Yasumori, I., 1996. J. Electroanal. Chem. 410 (2), 173–179.
Bambhania, H.M., Chakraborty, D., Wen, H., Barton, S.C., 2017. J. Electrochem. Soc. 164 (4), H232-H240.
Barus, C., Romanytsia, I., Striebig, N., Garçon, V., 2016. Talanta 160, 417–424.
Berchmans, S., Issa, T.B., Singh, P., 2012. Anal. Chim. Acta 729, 7–20.
Campbell, E.R., Warsko, K., Davidson, A.-M., Campbell, W.H., 2015. MethodsX 2, 211–218.

Chung, H.Y., Baek, B.S., Song, S.H., Kim, M.S., Huh, J.I., Shim, K.H., Kim, K.W., Lee, K.H., 1997. Age 20 (3), 127–140.
Duffy, G., Maguire, I., Heery, B., Nwankire, C., Ducrée, J., Regan, F., 2017. Sens. Actuators, B 246, 1085–1091.
d'Urso, E.M., Coulet, P.R., 1990. Anal. Chim. Acta 239, 1–5.
d'Urso, E.M., Coulet, P.R., 1993. Anal. Chim. Acta 281 (3), 535–542.
Ferri, S., Kojima, K., Sode, K., 2011. J. Diabetes Sci. Technol. 5 (5), 1068–1076.
Fiske, C.H., Subbarow, Y., 1925. J. Biol. Chem. 66 (2), 375–400.
Grand, M.M., Clinton-Bailey, G.S., Beaton, A.D., Schaap, A.M., Johengen, T.H., Tamburri, M.N., Connelly, D.P., Mowlem, M.C., Achterberg, E.P., 2017. Front. Mar. Sci. 4, 1–16.
Grattieri, M., Tucci, M., Bestetti, M., Trasatti, S., Cristiani, P., 2016. ChemElectroChem 3 (11), 1884–1889.
Gross, A.J., Chen, X., Giroud, F., Abreu, C., Le Goff, A., Holzinger, M., Cosnier, S., 2017. ACS Catal. 7 (7), 4408–4416.
Haemmerli, S.D., Suleiman, A.A., Guilbault, G.G., 1990. Anal. Biochem. 191 (1), 106–109.
Heller, A., 1990. Acc. Chem. Res. 23, 67–87.
Heller, A., Feldman, B., 2008. Chem. Rev. 108 (7), 2482–2505.
Jońca, J., Barus, C., Giraud, W., Thouron, D., Garçon, V., Comtat, M., 2012. Int. J. Electrochem. Sci. 7, 7325–7348.
Jońca, J., Giraud, W., Barus, C., Comtat, M., Striebig, N., Thouron, D., Garçon, V., 2013. Electrochim. Acta 88, 165–169.
Jońca, J., León Fernández, V., Thouron, D., Paulmier, A., Graco, M., Garçon, V., 2011. Talanta 87, 161–167.
Jovanovic, S., Steenken, S., Hara, Y., Simic, M.G., 1996. J. Chem. Soc. Perkin Tans. 2, 2497–2504.
Kinoshita, H., Yoshida, D., Miki, K., Usui, T., Ikeda, T., 1995. Anal. Chim. Acta 303 (2-3), 301–307.
Kothe, T., Pöller, S., Zhao, F., Fortgang, P., Rögner, M., Schuhmann, W., Plumeré, N., 2014. Chem. Eur. J. 20 (35), 11029–11034.
Kulys, J., Higgins, I.J., Bannister, J.V., 1992. Biosens. Bioelectron. 7 (3), 187–191.
Lee, J., Filosa, S., Bonvin, J., Guyon, S., Aponte, R.A., Turnbull, J.L., 2001. Protein Expr. Purif. 22 (2), 180–188.
Lopez, F., Zerria, S., Ruff, A., Schuhmann, W., 2018. Electroanalysis 30.
Male, K.B., Luong, J.H.T., 1991. Biosens. Bioelectron. 6 (7), 581–587.
Mano, N., Mao, F., Heller, A., 2003. J. Am. Chem. Soc. 125 (21), 6588–6594.
Mano, N., Mao, F., Heller, A., 2005. J. Electroanal. Chem. 574 (2), 347–357.
Martens, N., Hall, E.A.H., 1994. Anal. Chem. 66 (17), 2763–2770.
Martens, N., Hindle, A., Hall, E.A.H., 1995. Biosens. Bioelectron. 10 (3-4), 393–403.
Milton, R.D., Lim, K., Hickey, D.P., Minteer, S.D., 2015. Bioelectrochemistry 106 (Pt A), 56–63.
Nagao, A., Seki, M., Kobayashi, H., 1999. Biosci. Biotechnol. Biochem. 63 (10), 1787–1790.
Ohara, T.J., Rajagopalan, R., Heller, A., 1994. Anal. Chem. 66 (15), 2451–2457.
Pinyou, P., Ruff, A., Pöller, S., Ma, S., Ludwig, R., Schuhmann, W., 2016. Chem. Eur. J. 22 (15), 5319–5326.
Plumeré, N., 2013. Anal. Bioanal. Chem. 405 (11), 3731–3738.
Plumeré, N., Henig, J., Campbell, W.H., 2012. Anal. Chem. 84 (5), 2141–2146.
Prévoteau, A., Mano, N., 2012. Electrochim. Acta 68, 128–133.
Prévoteau, A., Mano, N., 2013. Electrochim. Acta 112, 318–326.
Quan, D., Shim, J.H., Kim, J.D., Park, H.S., Cha, G.S., Nam, H., 2005. Anal. Chem. 77 (14), 4467–4473.
Ruff, A., 2017. Current Opinion in Electrochemistry 5 (1), 66–73.
Schindler, D.W., 2012. Proc. R. Soc. B 279 (1746), 4322–4333.
Shao, M., Pöller, S., Sygmund, C., Ludwig, R., Schuhmann, W., 2013. Electrochem. Commun. 29, 59–62.
Smith, V.H., 2003. Environ. Sci. & Pollut. Res. 10 (2), 126–139.
Sokol, K.P., Mersch, D., Hartmann, V., Zhang, J.Z., Nowaczyk, M.M., Rögner, M., Ruff, A., Schuhmann, W., Plumeré, N., Reisner, E., 2016. Energy Environ. Sci. 9 (12), 3698–3709.
Tremey, E., Stines-Chaumeil, C., Gounel, S., Mano, N., 2017. ChemElectroChem 27, 2520–2526.
Tremey, E., Suraniti, E., Courjean, O., Gounel, S., Stines-Chaumeil, C., Louerat, F., Mano, N., 2014. Chem. Commun. 50 (44), 5912–5914.
Tsujimura, S., Murata, K., Akatsuka, W., 2014. J. Am. Chem. Soc. 136 (41), 14432–14437.
Wang, J., 2008. Chem. Rev. 108 (2), 814–825.
Wang, Y., Tong, L., 2010. Sens. Actuators, B 150 (1), 43–49.
Watanabe, E., Endo, H., Toyama, K., 1988. Biosensors 3 (5), 297–306.
Wittbrodt, B.T., Squires, D.A., Walbeck, J., Campbell, E., Campbell, W.H., Pearce, J.M., 2015. PloS one 10 (8), 1–17.
Wollenberger, U., Schubert, F., Scheller, F.W., 1992. Sens. Actuators, B 7 (1-3), 412–415.
Zhang, Y., Wilson, G.S., 1993. Anal. Chim. Acta 281 (3), 513–520.

Highlights

Second generation electrochemical phosphate biosensor

Bioelectrocatalytic-electrochemical cascade bypasses O_2 interferences

Phosphate quantification is possible in complex sample matrices

Practical point-of-use phosphate sensing even in the hands of non-trained users.